Robust Extraction of Wheel Region for Vehicle Position Estimation using a Circular Fisheye Camera

Kenichi Hirose†, ††, Takashi Toriu†† and Hiromitsu Hama††

†Department of Information Engineering, College of Industrial Technology, Hyogo, 661-0047 Japan
††Graduate School of Engineering, Osaka City University, Osaka, 558-8585 Japan

Summary
Vision-based research in driver support and traffic monitoring systems aiming for collision avoidance and for free traffic jams has attracted a lot of attention lately. In this paper, we propose a robust new extraction method of wheel region for estimating the vehicle position on a road taking the distortion in a circular fisheye image into consideration. In order to make the process more effective, Sobel edge detector is used after modification. Through experimental results, the effectiveness of our proposed method is confirmed.

Key words:
circular fisheye, wheel extraction, tire-road contact point, side view, distortion of projection system

1. Introduction

For driving safety in Intelligent Transport Systems (ITS), various types of support for improving vision, avoiding collisions, driving vehicle and so on, have been derived from information obtained from in-car device. In addition, the data on the various types of traffic-related fatalities show the largest proportion is from collisions that involve two or more vehicles[1], so it is especially important to detect close vehicles. We study the method for detecting vehicles close to driver's vehicle using a fisheye camera. While there have been many studies to display image information about the area around a vehicle using fisheye cameras[2][3], but also few studies to detect nearby vehicles and estimate their positions.

In the ultimate system configuration of our study, four fisheye cameras are assumed to be used. In this paper, we propose methods for extracting robust vehicle wheel regions on a circular fisheye image. After extracting the wheel regions from the vehicle side images acquired from the fisheye camera mounted on the driver's vehicle, tire-road contact points were detected. This detection of the contact points makes it possible not only to detect the vehicles, but can also lead to the estimation of vehicle positions, vehicle directions, and lengths of wheelbase. This can be very useful for preventing collisions while changing lanes, moving and parking a vehicle in a parking lot.

There are many works related to such applications as vehicle detection, position estimation [4-12]. However, nearly all of these studies have focused on front and rear views. There are relatively little works focused on side views, because it requires multiple cameras or a super wide angle lens to get a wide field of view. Other works similar to our study, where vehicles have been detected based on extracting wheels, include those by O. Achler et al. [9] and Y. Iwasaki et al.[10]. Those works have all extracted wheels based on background subtraction using normal fixed cameras. C. Lai et al.[11] have been estimated the vehicle position and detecting tire contact points. In their work, the wheel is supposed to be an ellipse, and is extracted on images acquired from a normal camera, and the tire-road contact points are detected. In our study with the fisheye camera, the wheel shape on image is not strictly an ellipse, but a distorted shape, so Lai et al.'s method cannot be used in our work. In addition, T. Gandhi et al.[12] effectively obtained a wide range information of vehicle sides using omni-directional cameras that gave panoramic view of surrounding. However, they are not designed for detecting close vehicles due to the characteristics of omni-directional cameras.

In this paper, we propose a robust new extraction method of vehicle wheel region taking the distortion in a circular fisheye image into consideration. In most cases where fisheye cameras are used, the images are transformed into normal images. However, we propose the method for extracting wheels directly from the fisheye image. In our method, we use the directional edge detection by expanded Sobel edge detector and the distortion parameters by considering projection system of fisheye camera. Through experimental results, the effectiveness of our proposed method is confirmed. In our method, because local features of the object vehicle such as wheel's edge detection is used, it can be used either with fixed cameras or vehicle-mounted cameras.

This paper is organized as follows. In section 2, we present the relations between the cameras and the vehicle. In section 3, we give a detailed description of the proposed method for extracting vehicle wheel region in a circular fisheye image. In section 4, we discuss the effectiveness of

Manuscript received December 5, 2009.
Manuscript revised December 20, 2009.

the proposed method based on the experimental results. Finally, we conclude the research results in last section.

2. The relations between the camera and vehicle

In the ultimate configuration of our system, four vehicle mounted fisheye cameras are assumed to be used. The relation between the fisheye cameras and the object vehicle is shown in Fig.1. The optic axis of cameras are parallel to the ground surface. The relation between the fisheye camera coordinate system and the image coordinate system is shown in Fig.2. The 3-dimensional spatial coordinate system of the fisheye camera is O-XYZ, and the image coordinate system is o-xy. If Z-axis is assigned as the optical axis, then x-axis and y-axis are set to be parallel to X-axis and Y-axis, respectively. A point ***P*** (*X*, *Y*, *Z*) in camera coordinates is shown as polar coordinates (ρ, θ, φ). As seen in the figure, this point is projected onto point ***p*** (r, ϕ) on the image. Here, Eq. (1) and (2) are established for the camera coordinate system and Eq. (3) and (4) are established for the image coordinate system.

$$\tan\varphi = \frac{X}{Y} \tag{1}$$

$$\tan\theta = \frac{\sqrt{X^2 + Y^2}}{Z} \tag{2}$$

$$r = \sqrt{x^2 + y^2} \tag{3}$$

$$\tan\phi = \frac{x}{y} \tag{4}$$

Here, $\varphi = \phi$. In addition, the following is generally used as the projection system of the fisheye camera.

$$\begin{aligned} r &= f\theta && \text{(Equidistance projection)} \\ r &= f\sin\theta && \text{(Orthographic projection)} \\ r &= 2f\tan(\theta/2) && \text{(Stereographic projection)} \\ r &= 2f\sin(\theta/2) && \text{(Equi-solid angle projection)} \end{aligned} \tag{5}$$

Here, f is the focal distance of the lens. For example, when a fisheye lens with an equi-solid angle projection system of a 180-degree angle of field is used, setting the angle of point ***P*** on the 3-dimensional space from the camera's optical axis at θ, the height r of the projection point ***p*** from the projection center ***o*** on the image plane can be expressed with the following equation:

$$r = \sqrt{2}R\sin\left(\frac{\theta}{2}\right) \tag{6}$$

Where, the constant R is the projection height when θ is set at 90 degrees and is the diameter of the circular image.

3. Our proposed method

Fig. 3 shows the diagram of wheel region extraction by our proposed method. Generally, in order to enhance stability of moving and lessen partial abrasion of tires, wheels are set with small angles such as toe angle, camber angle and so on, and they are not completely vertical to the road surface. However, since these angles are very slight, about one degree or so, the wheels in our work are assumed to be perpendicular to the road surface. In addition, since there are bumps, holes and so on a wheel surface, wheels are not perfectly plane. However, because their outlines resemble circles, it is assumed that their surfaces can be approximated into the planes.

Vehicle images taken with normal cameras have the following features:

a) The shape of the wheel region is circular or elliptical.
b) The tire section is nearly black.
c) The wheel section is somewhat brighter than the tire section.

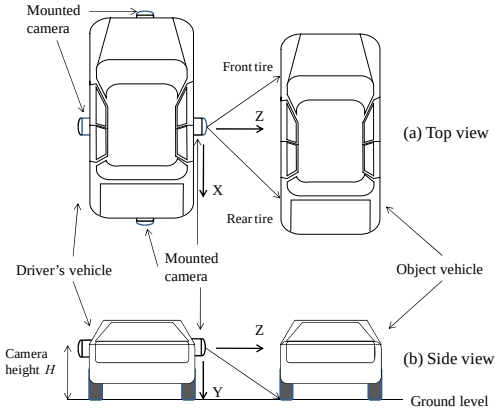

Fig. 1 The relation between the fisheye cameras and the object vehicle.

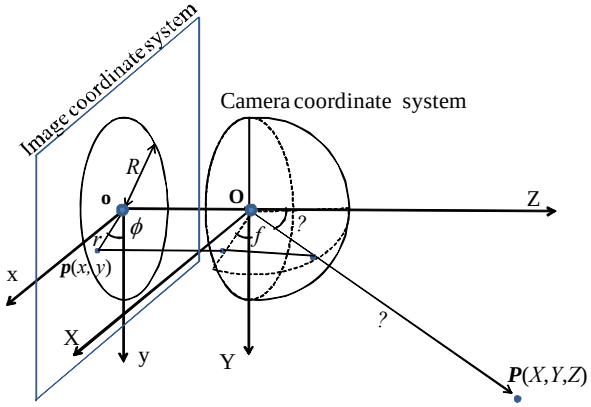

Fig. 2 The relation between the camera coordinate system and the image coordinates system.

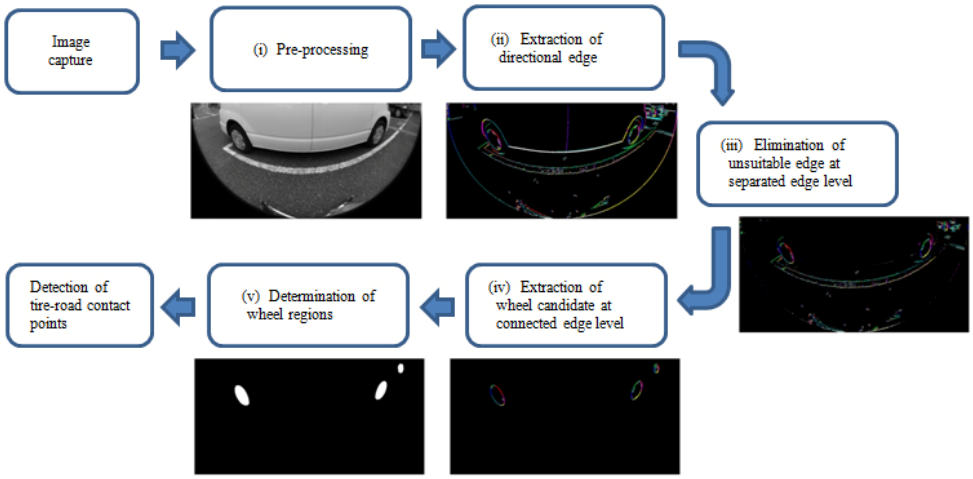

Fig. 3 The diagram of wheel region extraction by proposed method.

These features have been mainly used in previous works[8] for detecting wheel region. However, because we use the fisheye camera, the wheel shapes are not a simple circle or ellipse but instead include some distortion. In most cases where fisheye cameras are used, after the images are transformed into normal images, the wheels are extracted as circles or ellipses. Here, we propose a method for extracting wheels directly from fisheye images.

3.1 Distorted shape of wheel region

When setting on the height of the camera, the supposed radius of the wheel, the image size and the projection system of fisheye camera, distorted shape parameters of the wheel corresponding to the image position can be calculated as shown in Fig. 4. The parameters are centroid point, wide and height of bounding box, distortion angle. Then the parameter table for the image positions is prepared beforehand. This figure shows the distortion shape for a case where wheels having radius of 30cm, positioned with intervals of 50cm from the camera, were imaged from the camera height of 100cm vertically to the ground surface. The values of each parameter are only set at grid points at 50cm intervals on the road, the values at intermediate positions are derived from cubic spline interpolation based on image positions of the centroid point. Generally, the normal line of a wheel is not always parallel with the camera's optical axis, and there is sometimes a tendency to be inclined horizontally from the optical axis. However, the distortion angle of the vertical straight line at the contact point has no effect on the incline of the wheel surface. As for the height and width of bounding box, while the height is almost unaffected by its incline, the width is easily affected. Therefore, by giving a margin when setting conditions for width in extracting the wheel region, this method can be applied to extraction

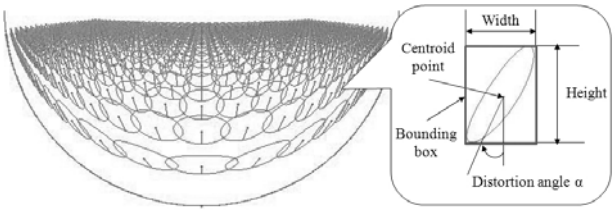

Fig. 4 The distorted shape on the image position and shape parameters.

even when the wheel surface is horizontally inclined to the camera's optical axis. In addition, while there are various radii of wheels, we adopt the average radius 30cm of the wheel of standard-sized car.

3.2 Extraction of wheel region

The wheel regions are extracted from the captured fisheye camera images, in the order of (i) to (v) in Fig. 3.

(i) Since wheels on a road are processed, the upper halves of the circular fisheye images are trimmed. In addition, to respond to changes in lighting conditions, gray levels of the whole image are normalized into 256 levels as 255 being the maximum gray level of the whole image.

(ii) Directional edges are detected using Sobel edge detector. First, as shown in the Fig. 5, the weighted averages of gray levels for the three neighboring pixels at both sides of a processed pixel, Ave_1 and Ave_2, are obtained using the edge detector, and the edge intensity SFV is calculated using Eq. (7).

$$SFV = \frac{(Ave_1 - Ave_2)}{Ave_1} \tag{7}$$

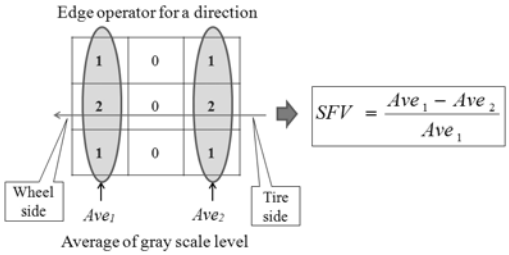

Fig. 5 Edge operator and calculation of edge intensity.

Where, Ave_1 is the average gray level for the pixels in the wheel section, and Ave_2 in the tire section. The edge intensity is calculated as SFV_i for each of eight directions. Above mentioned the wheel features b) and c) are the same even with a fisheye camera. The pixels that satisfy the following conditions (8) are detected as edge pixels:

$$\begin{cases} Ave_1 > T_1 \\ Ave_2 < T_2 \\ SFV > T_e \end{cases} \quad or \quad \begin{cases} Ave_2 > T_2 \\ \\ Ave_1 - Ave_2 > T_3 \end{cases} \tag{8}$$

where, $T_1 \sim T_3$ and T_e are the threshold values of the gray levels and edge intensity, respectively. Either right or left in conditions is used according to the brightness of the tire section. These values are determined by considering the relative brightness of the wheel section and the tire section. In our experiments, the values for $T_1 \sim T_3$ and T_e are 15, 100, 75 and 0.3, respectively. In these conditions, the left are applied to general lighting conditions, while the right are applied to so strong lighting conditions such as when sunlight directly shines on the wheel. In addition, within the edge intensity SFV_i of the eight directions, the direction i, with the maximum value is made the edge direction in the pixels, and the group of neighboring pixels having the same value is derived as the directional edge. Fig. 6 shows an example of extracting wheel edges based on directional edges. Directional edges, such as shown in Fig. 6 (b), are detected from the wheel image in Fig. 6(a). By eliminating unsuitable edges as the wheel outline from the directional edges (next steps (iii), (iv)), the wheel edge can be extracted, as shown in Fig.6(c).

(iii) To eliminate unsuitable edges, individual directional edges are processed. First, the bounding box for the centroid of a target edge is derived from parameter table, and the box is estimated as rectangular region containing the wheel. The bounding box of the target edge itself is compared with this estimated region, and the edges that satisfy the following conditions are eliminated:

- The height of bounding box is higher than the height of estimated region.
- There are not four types of directional edges within the estimated region.

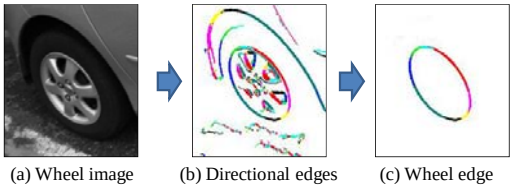

Fig. 6 Wheel extraction by directional edges.

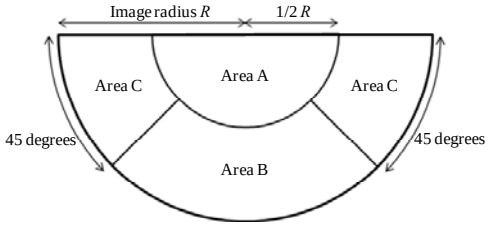

Fig. 7 Division of semicircular image for wheel extraction.

- When setting the direction of a target edge as i, there do not exist directional edges of i-1 and i+1 at either of the ends.

(iv) To extract candidate wheel regions, multiple neighboring directional edges are processed as one group edge. When edges are discontinuous, dilation of morphological processing is done in response to the edge direction, and contiguous edges are considered as a uniform group. By assuming this group edge formed part of the wheel region, the estimated region of the wheel is derived from parameter table in a similar way to step (iii). Here, semicircular image is divided into three areas as shown in Fig. 7. The ratio of height to width on distorted circular shape nearly equals 1 in area A, is lower in area B and is higher in area C. Therefore, in addition to the comparisons of bounding box height above mentioned, the judgments are made regarding the size relation between height and width of estimated region for these areas, and whether or not the absolute of incline angle of the principal axial is at least 40 degrees in area C. Furthermore, the wheel region is composed of various types of directional edges, so group edge regions comprise of at least five types of directional edges become candidate wheel region.

(v) To determine wheel region, the processes involves dilation in response to edge direction, filling the inside of the edge region, and opening processing of morphological processing, carried out in order. The missing sections of wheel regions are filled in, and excess edge sections are eliminated. Here as well, the candidate regions that are suitable after comparison with the region estimated from the parameter table are determined as the wheel.

As the following step, using the method in our previous work[13], the tire-road contact points are detected using profiles of gray levels based on the wheel region, and the wheel positions on road are estimated as vehicle positions.

4. Experimental Results and Discussion

In order to verify the effectiveness of the proposed method, experiments of the wheel extraction and tire-road contact point detection were conducted. The fisheye cameras consisted of a circular fisheye lens (SIGMA 4.5mmF2.8EX DC CIRCULAR FISHEYE HSM: angle of view is 180-degree, projection system is equi-solid) mounted on a digital still camera (Canon EOS Kiss Digital N, 3456×2304 pixels). Using a fisheye lens of relatively high accuracy, fixed values of the radius and central position of the circular images were set beforehand. The camera's optical axis was set to be parallel to the ground, and the camera was mounted on a tripod at a height of 100cm. The captured images were processed by trimming them into rectangular region of 1170 × 585 pixels including semicircular fisheye image, the resolution per unit viewing angle is 6.5 pixel/degree. Side images of vehicles that were parked in a parking lot were targeted within position range as shown in Fig. 8. Images were taken under various weather conditions, such as fine, cloud, and rain.

The results of detecting tire-road contact points and the process of extracting wheel regions under various conditions are shown in Fig. 9. The left images in this figure are the detection results of contact points, and the right images on divided into top and bottom show the process of extracting. The upper parts of the right images show, from left, normalized gray levels, edge detection, and wheel extraction. While the bottom parts show the process for detected rectangular regions of the wheels, from right, the detected wheel regions, images after gamma conversion, and detection of tire-road contact points, with the red and yellow dots showing the wheel's centroid and the tire-road contact points, respectively. From these figures, it can be seen that the contact points were correctly detected, regardless of vehicle size, position and so on.

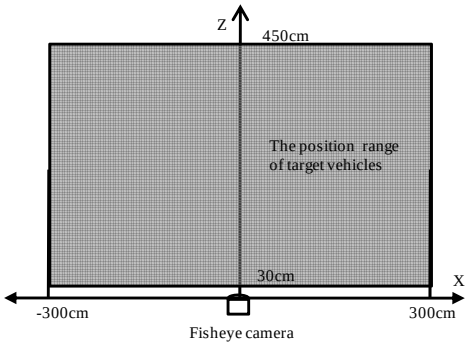

Fig. 8 The position range of target vehicles from fisheye camera.

Fig. 9(a) to (d) show detection results under four kinds of weather conditions: fine day with sunlight from the back and the front, cloudy day, and rainy day, respectively. As a result of making two contrast adjustments and by changing conditions for threshold in the edge detection, contact points were correctly detected even in cases such as (a) where the tire was exposed to direct sunlight and (b) where the tire was strongly shaded from sunlight (backlight). It is found that our method can be used even when there are changes in brightness according to the position of the sun. And it was also possible to detect contact points even where road surfaces have low gray levels on rainy days, such as in (d).

Fig. 9(e) shows the result for cases where the wheel surface was inclined horizontally to the camera's optical axis. It can be seen that the contact points were correctly detected. This result suggests that the proposed method is robust even to the incline of the wheel surface.

Table 1 shows the results of wheel extraction. In this table, some points were not extracted, but no points were extracted by mistake, and the wheels were extracted in about 97% of the target images. As this result, the effectiveness of the vehicle detection was demonstrated.

Fig. 10 shows an example of unsuccessful wheel extraction. The main reason for not extracted was failure at the step of detecting the directional edge. As shown in (a), when the vehicle position Z from the camera is an extremely close and the wheel position $|X|$ from the camera is large, there is great distortion of the wheel in the circumferential parts on the fisheye image. Then the tire section which is outside the wheel section sometimes does not appear on the image. So, directional edges were not detected and the wheel was not extracted. And, as shown in (b), for vehicle with low-profile tires, the wheel was not extracted when $|X|$ was large. In addition, when $|X|$ was extremely large and the wheel was imaged in the circumferential parts on the circular image, the wheel shape became extremely oblong and no roundness. In such cases, because there were not many kinds of directional edges detected, they were judged to be removable target edges. However, as shown in (c), when $|X|$ of one wheel was small, this wheel was correctly extracted, so it was possible to use this information to detect vehicles. Furthermore, when Z were small and $|X|$ were large for both wheels, the probability of non-extraction greatly increased. However, since four direction fisheye cameras are envisioned for the ultimate system configuration of our research, it should be possible to detect a vehicle with another camera faced a different direction.

More, Table 2 shows the results of position estimates using tire-road contact points. This table lists the average and standard deviation of errors between the position X, Z estimated from the detected points and actual measurement values on the road. The sixty images of nine vehicles were processed. These show the results for supposed tire radii of

(a) Fine day 1(Sunlight from the back).

(b) Fine day 2(Sunlight from the front).

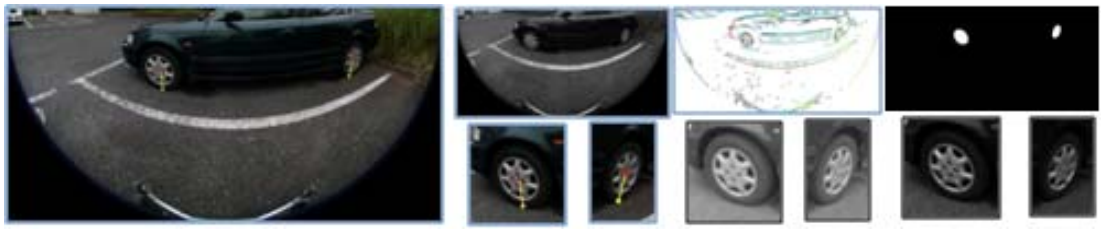

(c) Cloudy day.

(d) Rainy day.

(e) Oblique wheel.

Fig. 9 Results of extraction of wheel regions and detection of tire-road contact points

Table 1 Results of wheel extraction.

Number of images	Two wheels extracted	One wheel extracted	Not extracted
208	140	61	7

Table 2 Results of comparative tests related to position estimation. (Ave.: Average, Std.: Standard deviation)

Tire radius	Error of position X [cm]		Error of position Z [cm]	
	Ave.	Std.	Ave.	Std.
30cm	4.4	3.4	4.6	3.6
40cm	4.6	3.5	4.6	3.7

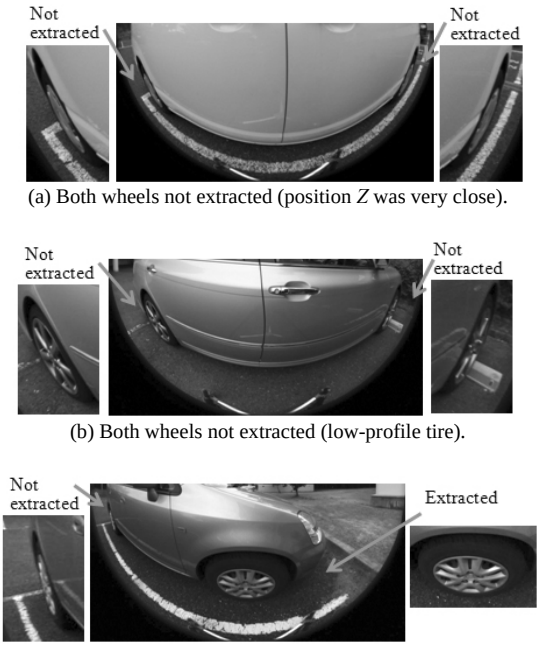

(a) Both wheels not extracted (position *Z* was very close).

(b) Both wheels not extracted (low-profile tire).

(c) One wheel extracted (position *X* was small).

Fig. 10 Examples of not extracted wheels.

30cm and 40cm in the calculations of distorted shape parameters. While actual measurements of tire radii of the test vehicles ranged from 26.5 to 32cm, the results were about the same. So it was confirmed that the differences in supposed wheel radii had almost no effect on detection. The results showed an average of not more than 5cm and deviation of not more than 4cm for both positions *X* and *Z*, and excellent results were obtained.

And there is other method with a fisheye camera that wheel regions are extracted as circle or ellipse after a pinhole image transformation. In this method, the prediction of the wheel position is needed extra to improve extraction, and it is necessary to transform the pinhole image whenever a fisheye image is captured. In proposed method, the calculation of the parameters table is needed once as initial processing, and this calculation time is about twentieth of pinhole transformation. Therefore, it is thought that proposed method can be good in the processing time.

5. Conclusion

In this paper, we have proposed a method for robust extracting wheel region from side images of vehicles using circular fisheye camera and its effectiveness has been experimentally confirmed. In images taken the wheel and the tire sections, wheel regions were extracted regardless of vehicle direction or weather conditions. In addition, since the error average of position estimation error based on extracted wheel region was not more than 5cm, it appears that these results were enough accurate. Therefore, we conclude that this method can be used to various applications for collisions avoidance, such as detecting other vehicles in a parking lot, or measuring the distance from a parked vehicle or the distance between vehicles moving side by side.

However, in cases where vehicles are extremely close or very far apart, this method should be used in conjunction with other methods. A future work will be to construct a comprehensive system that includes linkages with multiple fisheye cameras and processing in real-time.

Acknowledgment

This work was supported by KAKENHI 19500162 Grant-in-Aid for Scientific Research (C).

References

[1] "White Paper on Traffic Safety in Japan," (in Japanese), Cabinet Office, Government of Japan, http://www8.cao.go.jp/koutu/taisaku/index-t.html

[2] X. Ying and Zhanyi Hu, "Distortion Correction of Fisheye Lenses using a Non-Parametric Imaging Model," Proc. Asian Conference on Computer Vision (ACCV 04), Jeju, Korea, pp.527-532, 2004.

[3] S. Li, "Monitoring Around a Vehicle by a Spherical Image Sensor," IEEE Trans. Intelligent Transportation System, 7, 4, pp.541-550, 2006.

[4] Z. Sun, G. Bebis and R. Miller, "On-Road Vehicle Detection: A Review", *IEEE Trans. Pattern Analysis and Machine Intelligence*, Vol. 28, No. 5, pp.694-711, 2006.

[5] S. J. Velat, J. Lee, N. Johnson and C. D. Crane III, "Vision Based Vehicle Localization for Autonomous Navigation", *Proceedings of the 2007 IEEE International Symposium on Computational Intelligence in Robotics and Automation*, Jacksonville, FL, USA, pp.528-533, June 2007

[6] L. Zhi-fang and Y. Zhisheng, "A Real-time Vision-based Vehicle Tracking and Traffic Surveillance", *Proceedings of the Eighth ACIS International Conference on Software Engineering, Artificial Intelligence, Networking, and Parallel/Distributed Computing*, pp.174-179, 2007

[7] C. R. Wang and J. J. Lien, "Automatic Vehicle Detection Using Local Features-A Statistical Approach", *IEEE Trans. Intelligent Transportation System*, Vol. 9, No. 1, pp.83-96, 2008.

[8] S. Sakuma, Y. Takahashi, A. Shio and S. Ohtsuka, "Vehicle Counter System Using Panoramic Images" (in Japanese), *Trans. of IEICE*, Vol.J85-D-II, No.8, pp. 1361-1364, 2002.

[9] O. Achler and M. M. Trivedi, "Camera Based Vehicle Detection, Tracking, and Wheel Baseline Estimation Approach", *IEEE Intelligent Transportation Systems Conference*, Washington, D.C., pp.743-748 , Oct. 2004.

[10] Y. Iwasaki and Y. Kurogi, "Real-time Robust Vehicle Detection through the Same Algorithm both Day and Night", *Proc. of the 2007 International Conference on Wavelet Analysis and Pattern Recognition*, Beijing, China, pp.1008-1014, Nov. 2007.

[11] C. Lai and W. Tsai, "Location Estimation and Trajectory

Prediction of Moving Lateral Vehicle Using Two Wheel Shapes Information in 2-D Lateral Vehicle Images by 3-D Computer Vision Techniques", *Proc. the 2003 IEEE International Conference on Robotics & Automation*, pp.881-886 ,2003.

[12] T. Gandhi and M. M. Trivedi, "Vehicle Surround Capture: Survey of Techniques and a Novel Omni-Video-Based Approach for Dynamic Panoramic Surround Maps", *IEEE Trans. Intelligent Transportation System*, Vol. 7, No. 3, pp.293-308 , 2006.

[13] K. Hirose, T. Toriu and H. Hama, "Detection of Tire-Road Contact Point for Vehicle Position Estimate: Considering Shape Distortion in a Circular Fisheye Image", Proc. 2009 the fifth International Conference on Intelligent Information Hiding and Multimedia Signal Processing, Kyoto, Japan, pp.178-181, Sept. 2009.

Kenichi Hirose received the M.E. degrees, in Engineering from Osaka City University. He is a doctoral candidate in Osaka City University, Japan. He is currently an associate professor at College of Industrial Technology. His research interest include ITS (Intelligent Transportation Systems), computer vision, computer graphics. He is a member of IEEE, ACM, IEICE, IPSJ, ISCIE and JSGG.

Takashi Toriu received the Dr. Sci. degrees in Physics from Kyoto University, Japan. He is currently professor at Osaka City University. His research interests include image processing, computer vision, mechanism of visual attention. He is a member of IEEE, IEICE, IIITE, IPSJ, IEEJ, JSAI and RSJ.

Hiromitsu Hama received the Dr. Eng. degrees in Electrical Engineering from Osaka University, Japan. He is currently emeritus professor at Osaka City University. His research interests include ITS (Intelligent Transportation Systems), 3D world reconstruction, computer vision, picture processing/understanding and multi-media search engine. He is a member of IEEE, IEICE, IIITE and J-FACE.